An Investigation of Gold Adsorption from a Binary Mixture with Selective Mesoporous Silica Adsorbents

Koon Fung Lam,[†,‡] King Lun Yeung,*[,‡] and Gordon McKay[‡]

Environmental Engineering Program and the Department of Chemical Engineering, Hong Kong University of Science and Technology, Clear Water Bay, Kowloon, Hong Kong, P.R. China

Received: September 30, 2005; In Final Form: December 5, 2005

Gold-selective adsorbents were prepared from mesoporous MCM-41 silica by grafting organic amine groups (i.e., RNH_2, R_2NH, and R_3N; R = propyl). NH_2-MCM-41, NRH−MCM-41, and NR_2-MCM-41 displayed strong affinity for gold and at 1 mmol/g loading adsorbed 0.40, 0.33, and 0.20 mmol/g of gold. Copper and nickel were not adsorbed on these adsorbents. Grafting surface chemical moieties introduces heterogeneity on an otherwise uniform MCM-41 pore surface and metal adsorption is best described by the Freundlich adsorption model. A series of binary adsorption equilibrium studies with NH_2-MCM-41 containing 2.2 mmol RNH_2/g shows that NH_2-MCM-41 adsorbs only gold from solutions containing copper and nickel with an adsorption capacity of 0.6 mol of Au/mol of RNH_2 (1.1 mmol of Au/g of NH_2-MCM-41). Copper and nickel were not adsorbed by NH_2-MCM-41 regardless of the solution concentration, composition, and pH (i.e., 2 to 4) in the presence of gold. The LeVan and Vermeulen adsorption model based on a single component Freundlich isotherm and corrected for the anion effect accurately predicted the binary adsorptions. The adsorbed gold was completely recovered by a simple acid wash and the recovered gold solution is 99% pure. The regenerated NH_2-MCM-41 remained 100% selective for gold removal and exhibited the same adsorption capacity even after several uses.

Introduction

Many chemical reactions and separations[1,2] were shown to benefit from the large surface area and well-defined pore structure of ordered mesoporous materials (e.g., M41S, FSM, HMS, and SBA). The use of ordered mesoporous materials as catalyst or support for homogeneous catalyst forms the basis of many new "green" synthesis routes for high-value chemicals and pharmaceuticals.[3] The recent work of Hata and co-workers[4] successfully established the value of mesoporous materials for chemical separation. They showed that the anticancer drug Taxol could be recovered at high purity from the extraction solvent using mesoporous silica with tailored pore structure. Besides their use for chemical syntheses and separations, ordered mesoporous materials also find application in environmental remediation. The early work of Feng et al.[5] showed that mercapto-functionalized MCM-41 are effective adsorbents for the removal of mercury and other heavy metals from water, and more recently Ho and co-workers[6] showed that MCM-41 can be chemically tailored to selectively adsorb, separate, and remove dyes from aqueous mixtures.

Although further cost reduction is needed for the economical use of mesoporous materials to general environmental problems, there are many specific cases where this technology is urgently needed. Metal-contaminated wastewater is a common problem in mining, electroplating, and electronic industries.[7] Most metals have adverse environmental effects that can cause long-term damage to soil and aquatic flora and fauna.[8] The health and ecological impacts of heavy metals are well documented. Heavy metals are toxic, carcinogenic, mutagenic, and often teratogenic.[9,10] Once released into the environment, they tend to accumulate in the food chain and persist in the environment for a long time.[11] Besides health and environmental reasons, there is a strong economic motivation for the removal and recovery of expensive, heavy metals from process water for recycle and reuse. Following the report of selective mercury adsorption with thiolated MCM-41 by Feng et al.,[5] other thiolated mesoporous silicas including SBA-15 and MCM-48 were also shown to be selective for mercury adsorption.[12−14] The removal of arsenate and chromate ions from drinking water was demonstrated by using metal-chelated ligands immobilized on mesoporous silica.[15] SBA-15 grafted with imidazole-containing chemical groups were reported to be highly selective for Pt^{2+} and Pd^{2+} ions and can separate these metals from solutions that also contain Ni^{2+}, Cu^{2+}, and Cd^{2+}.[16]

This work describes the preparation of selective and regenerable MCM-41 adsorbent for facile removal and recovery of high-purity gold from binary mixtures containing copper and nickel. The MCM-41's simple cylindrical pore geometry and high degree of pore symmetry afford an easier mathematical description and its amorphous pore wall is a good approximation of an ideal Langmuir surface. Introducing well-defined surface functional groups onto the pore wall gives an excellent opportunity to study the effects of site interactions on adsorption capacity and selectivity. The effects of pH, metal concentration, and composition on binary component adsorption were investigated and the results were perfectly described by using a simple adsorption model based on single-component adsorption data. The recovery of high-purity gold and the regeneration of spent adsorbents were also studied in detail.

* Author to whom correspondence should be addressed. Phone: 852-2358-7123. Fax: 852-2358-0054. E-mail: kekyeung@ust.hk.
† Environmental Engineering Program.
‡ Department of Chemical Engineering.

10.1021/jp055577n CCC: $33.50
Published on Web 01/13/2006

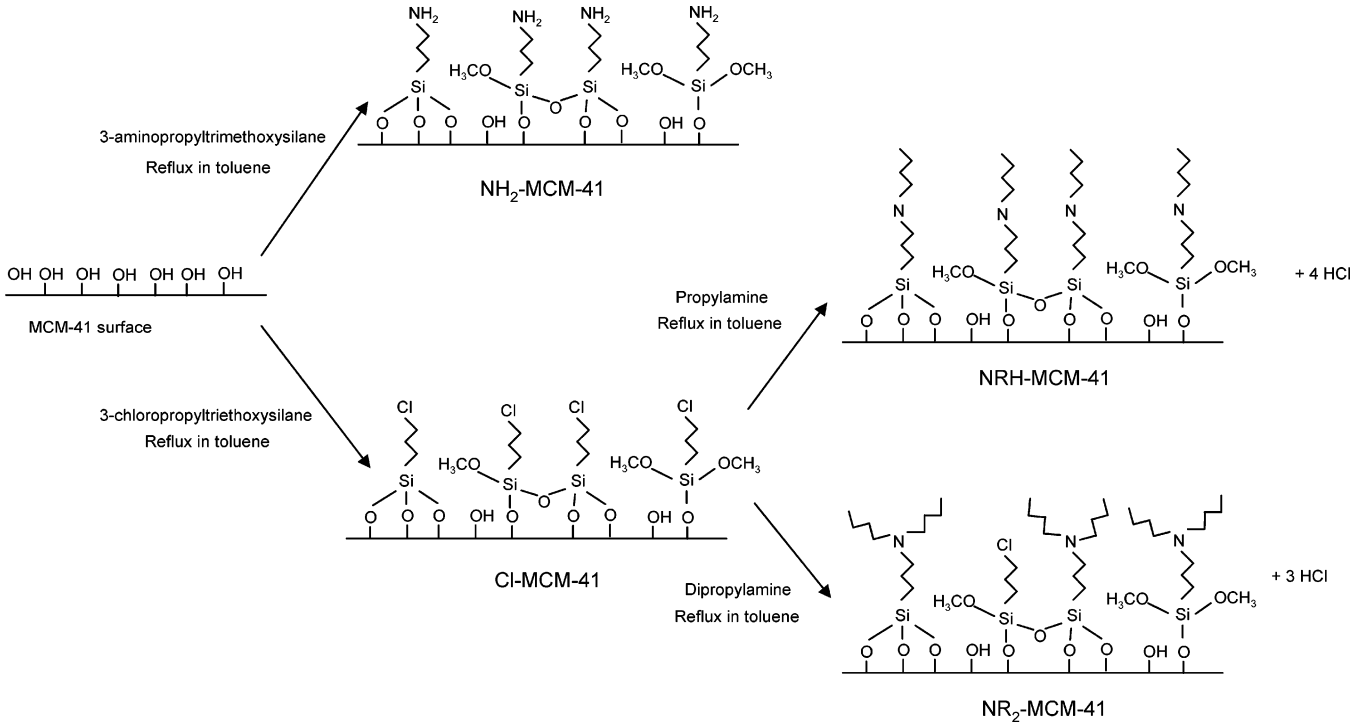

Figure 1. Scheme for grafting organic amines on the surface of MCM-41.

Experimental Section

Synthesis and Characterization of MCM-41 Adsorbents. MCM-41 powder was prepared from an alkaline synthesis solution containing tetraethyl orthosilicate (TEOS, 98%, Aldrich), cetyltrimethylammonium bromide (CTABr, 99.3%, Aldrich), and ammonium hydroxide (NH_4OH, 28−30 wt %, Fisher Scientific) at a molar ratio of 6.58 TEOS:1 CTABr:292 NH_4OH:2773 H_2O. The synthesis was conducted at room temperature under vigorous mixing to obtain well-dispersed, micron-sized particles. The MCM-41 was filtered, washed, dried, and ground to obtain free flowing powder. The powder was collected and calcined in a single batch at 823 K for 24 h to burn away the organic templates. The particle size distribution of MCM-41 was determined by scanning electron microscopy (SEM, JEOL JSM 6300F). A detailed description of the particle morphology and pore structure was obtained by using a high-resolution, transmission electron microscope (TEM, JEOL JEM 2010), while the average surface area and pore size were calculated from nitrogen physisorption experiments (Coulter SA 3100) and X-ray diffraction data (XRD, Philips 1830).

Different nitrogen-containing organic moieties, RNH_2, R_2NH, and R_3N (where R is a propyl group), were grafted on MCM-41 following the schemes depicted in Figure 1. Aminopropyl groups were added by reflux in a dry toluene solution containing 0.4 M 3-aminopropyltrimethoxysilane (97%, Aldrich) at 383 K for 18 h. The adsorbent was recovered after a series of centrifugation and washing steps. Different amount of aminopropyl groups (i.e., 0.34 to 2.26 mmol/g) were grafted by simply changing the precursor concentration. The propylamino and dipropylamino groups were prepared by first grafting chloroproyltriethoxysilane (0.4 M, 95%, Aldrich) onto the MCM-41 by reflux in dry toluene at 383 K for 18 h (Figure 1). The powder was recovered by centrifugation, dried, weighed, and resuspended in a dry toluene solution containing 0.4 M propylamine (or dipropylamine). The conversion was conducted under reflux at 383 K for 18 h. The consequent change in surface area and pore structure after modification was examined by nitrogen physisorption and X-ray diffraction. Thermogravimetric and differential thermal analyses (TGA/DTA, Setaram 31/1190) were conducted to identify and quantify the numbers of organic moieties grafted on the MCM-41. The samples were heated in 25 sccm dry air from 298 to 973 K at 5 deg/min and the resulting weight loss and heat flow were recorded. X-ray photoelectron spectroscopy (XPS, Physical Electronics PHI 5000) and Fourier transform infrared spectroscopy (FTIR, Perkin-Elmer GX 2000) were used to determine the surface composition and chemistry of the adsorbent materials.

Adsorption and Separation Experiments. Single-component adsorption isotherms of gold, copper, and nickel were measured by using 0.1 g of adsorbent for 100 mL of aqueous solutions containing 0.5 to 4 mM metal ions. Gold(III) chloride (99%, Aldrich), copper(II) chloride (98%, Aldrich), and nickel(II) nitrate hexahydrate (99%, Aldrich) were used to prepare the metal salt solutions. The pH of the solutions was adjusted to 2.5 ± 0.02 by adding a small amount of dilute hydrochloric acid. The batch adsorption experiments were conducted in a shaker bath kept at a constant temperature of 295 ± 2 K. The concentration of metals in the solution was analyzed by inductively coupled plasma, atomic emission spectrometer (ICP-AES, Perkin-Elmer Optima 3000XL). Each sample was measured twice and the results averaged. Calibration was made before each set of measurements with use of ICP standards solutions, 1000 ppm of Au (99.999%) in 2% HCl, 1000 ppm of Cu (99.999%) in 2% HNO_3, and 1000 ppm of Ni (99.99%) in 2% HNO_3, purchased from High-Purity Standards.

Binary $AuCl_3/CuCl_2$ and $AuCl_3/Ni(NO_3)_2$ solutions of different metal ion concentrations and pH were prepared for selective adsorption studies. In the adsorption experiments, 0.1 g of adsorbent powder were added to the 100 mL solution and allowed to reach an equilibrium at a temperature of 295 ± 2 K. The remaining metal ions in the solution after adsorption were measured by ICP-AES, which permits simultaneous analysis of up to 40 elements. Three measurements were averaged and the equilibrium adsorption capacity calculated. X-ray photoelectron spectroscopy was used to confirm the adsorption of metals on the adsorbent powders. The binary component

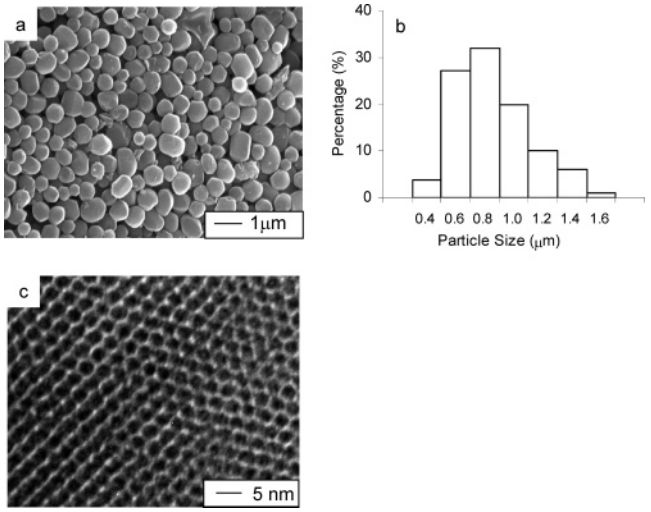

Figure 2. (a) Scanning electron microscope picture and (b) particle size distribution of MCM-41 powder. (c) A high-magnification TEM picture showing the characteristic hexagonal pore structure of MCM-41.

adsorption was also monitored with time to investigate the adsorption kinetics.

Gold Recovery and Adsorbent Regeneration. The recovery of adsorbed gold and the regeneration of spent adsorbent were investigated for NH_2-MCM-41 adsorbent. A 20 mg sample of adsorbent was used to remove gold from a 16 mL of solution containing 3 mM $AuCl_3$ and 3 mM $CuCl_2$. The adsorption lasted for 1 h at room temperature and a pH of 2.5. The adsorbent was then recovered by centrifugation and washed with 3 mL of 5.2 M HCl solution. The amounts of adsorbed and recovered metals were determined by ICP-AES measurements. The experiment was repeated five times to investigate the effects of the regeneration process on the adsorption properties of NH_2-MCM-41.

Results and Discussion

Adsorbent Preparation and Characterization. Each batch of synthesis produced about 20 g of MCM-41. The quality of the recovered powder was monitored by X-ray diffraction and light-scattering experiments. Although the powder crystallinity and particle size of each batch rarely differs by more than 20%, the products of several batches were mixed and blended together to further improve homogeneity. This is important to ensure reproducibility in subsequent adsorbent preparation. The collected powder was calcined in air at 823 K for 24 h to remove the template molecules (i.e., CTA^+). Figure 2a shows a scanning electron microscope picture of the calcined MCM-41 powder. The MCM-41 particles are flat and have a hexagonal-to-round shape resulting in a disklike morphology. It is evident from the micrograph that the particles have a uniform size. Indeed, measurements show that the powder has a narrow particles size distribution (Figure 2b). The MCM-41 has an average particle diameter of 0.8 ± 0.4 μm and a thickness of about 0.1 μm. The dry, calcined powder is free flowing and has little tendency to agglomerate. The high-resolution transmission electron micrograph of the calcined MCM-41 revealed a highly ordered, hexagonal pore structure (Figure 2c). Table 1 lists the BET surface area measured by N_2 physisorption, the average pore size calculated from XRD and N_2 physisorption experiments, and the predominant surface moieties detected by FTIR.

Three adsorbents were prepared by grafting RNH_2, RNRH, and RNR_2 groups on calcined MCM-41 powder according to Figure 1. XPS analysis indicated the presence of unreacted methoxys in the grafted functional groups. Table 2 shows the C/N atomic ratios for the different surface function groups. The values suggest that less than 20% of the methoxy groups remained unreacted. The NRH-MCM-41 and NR_2-MCM-41 were prepared by reacting the chloropropyl-grafted MCM-41 with 50× excess propylamine and dipropylamine reactants. The XPS did not detect any Cl atoms on NRH-MCM-41 but trace amounts were found on the NR_2-MCM-41. This means that all chloropropyl groups were converted in NRH-MCM-41 and less than 2% remained unreacted in the NR_2-MCM-41. The latter is because of the stearic effects from the bulky dipropylamine. The substitution of the propyl group for hydrogen of the amine is expected to cause steric hindrance and affect the electronegativity of the nitrogen center resulting in a change in adsorption properties.

X-ray diffraction in Figure 3a shows that grafting organic moieties onto the MCM-41 introduces disorder. The BET surface area decreases from 1070 m^2/g to 770 m^2/g after grafting RNH_2 groups on MCM-41 with a concomitant decrease in pore size from 30.9 Å to 29.2 Å. The FTIR spectrum of the MCM-41 in Figure 3b displays the characteristic bands for silanol groups at 3675, 950, and 800 cm^{-1}, while NH_2-MCM-41 gave IR absorbance peaks at 3360 cm^{-1} together with 3288 and 1600 cm^{-1} corresponding to the $-NH_2$ and C−N groups, respectively. The attachment of the aminopropyl groups on surface silanols is responsible for the disappearance of the characteristic absorbance peaks of silanol in the NH_2-MCM-41 sample. Table 1 summarizes the physical and chemical properties of MCM-41, NH_2-MCM-41, NRH-MCM-41, and NR_2-MCM-41 adsorbents.

Thermogravimetric and differential thermal analyses (TGA/DTA) are established techniques for monitoring the adsorbent preparation. The amount of organic moieties grafted on the

TABLE 1: Physical and Chemical Properties of the Mesoporous Silica Adsorbents

						adsorption capacity at pH 2.5, mmol/g (mg/g)		
	surface area, m^2/g	pore size,[a] nm	moiety	characteristic FTIR signals, cm^{-1}	loading of functional groups,[b] mmol/g	Au^{3+}	Cu^{2+}	Ni^{2+}
MCM-41	1070	3.09	OH	3675 (O−H)		0	0	0
NH_2-MCM-41	774	2.92	NH_2	3360 and 3288 (N−H),	2.26	1.40 (275)	0	0
NH_2-MCM-41	772	2.82	NH_2	1600 (C−N)	1.01	0.40 (79)	0	0
NRH−MCM-41	911	2.83	RNH	2973 and 2865 (*n*-propyl), 1500 ($CH_2-NH-CH_2$)	1.01	0.33 (65)	0	0
NR_2-MCM-41	889	2.79	NR_2	2973 and 2865 (*n*-propyl), absence of OH and N−H	0.94	0.20 (40)	0	0

[a] Pore size was calculated based on XRD, BET surface area, and pore volume.[17] [b] Amount was calculated from thermogravimetric experiment.

TABLE 2: Atomic C/N Ratios of the Prepared Adsorbents

		C/N ratio	
	functional group	theoretical	XPS
NH_2 (2.26 mmol/g)	$CH_2CH_2CH_2NH_2$	3	3.38
NH_2 (1.01 mmol/g)	$CH_2CH_2CH_2NH_2$		3.62
NRH (1.01 mmol/g)	$CH_2CH_2CH_2NCH_2CH_2CH_3$	6	6.51
NR_2 (0.94 mmol/g)	$CH_2CH_2CH_2NH(CH_2CH_2CH_3)_2$	9	8.89

MCM-41 is determined from the weight loss of the sample during thermogravimetric analysis (Figure 3c). For the NH_2-MCM-41 adsorbent, the weight losses in regions I and II are due to the desorption of moisture and hydrogen-bonded water molecules from the adsorbent. These processes are endothermic and are associated with a negative heat flow of 131 J/g in the DTA graph. The weight loss in region III is exothermic and is due to the oxidation of the grafted surface functional groups. This weight loss was used to calculate the amount of functional moieties attached to the adsorbent. Also, the DTA graph of this region are unique and can be used to assess the reproducibility of the adsorbent preparation.

Single-Component Adsorption. Figure 4 plots the gold adsorption isotherms for MCM-41, NH_2-MCM-41, NRH-MCM-41, and NR_2-MCM-41. To allow for comparison, the same number of functional groups (ca. 1 mmol/g) were grafted on NH_2-MCM-41, NRH-MCM-41, and NR_2-MCM-41 as shown in Table 1. The adsorption was fast and equilibrium was reached in less than 30 min because of the easy access through the large cylindrical pores of the mesoporous silica. The results show that gold does not adsorb on MCM-41, indicating that gold has

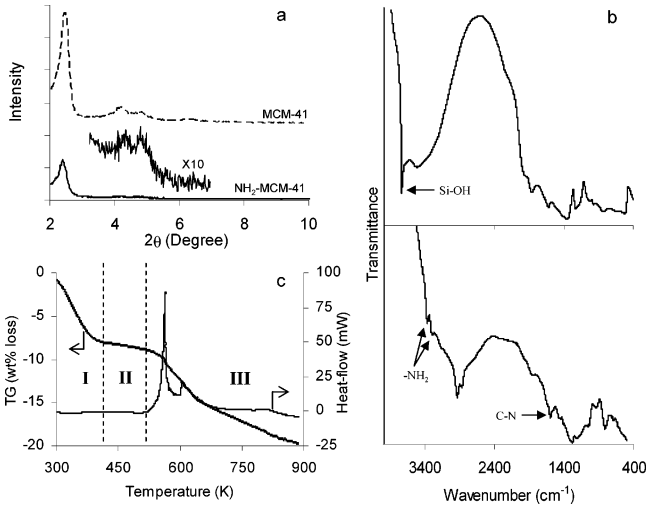

Figure 3. (a) XRD, (b) FTIR, and (c) TGA/DTA analyses of the MCM-41 and NH_2-MCM-41 samples.

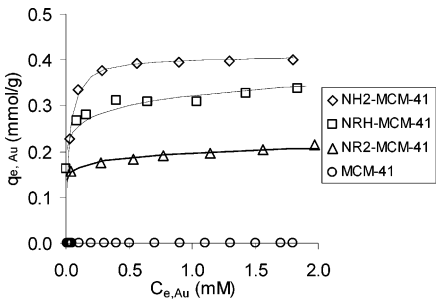

Figure 4. Single component gold adsorption isotherms of MCM-41, NH_2-MCM-41, NRH-MCM-41, and NR_2-MCM-41 (0.1 g of adsorbent per 100 mL of solution, pH 2.5, and $T = 295 \pm 2$ K). Please note the symbols represent experimental data and the lines represent model calculation.

TABLE 3: Adsorption Capacity for Gold of Different Common Adsorbents[a]

adsorbent	max adsorption capacity, mmol/g (mg/g)	ref
NH_2-MCM-41 (2.2 mmol NH_2/g)	1.40 (275)	this work
NRH-MCM-41 (1.01 mmol NRH/g)	0.33 (65)	this work
NR_2-MCM-41 (0.94 mmol NR_2/g)	0.20 (40)	this work
activated carbon	0.18 (35)	18
Degusorb C25 (granular cocnonut-shell carbon)	0.5 (100)	19
commercial carbon (PICA G210 AS)	0.51 (100)	20
Bagasse	1.16 (229)	20
polymers with sulfur-containing functional groups	0.4−6.5 (79−1280)	21
anionic Purolite A-100	2.53 (500)	22
rice husk ash	0.11 (22)	23
cationic exchange resin	∼1.23 (243)	24
different resins with amine, thiol, and amine-mercaptan functionalities	2.2 (433)	25

[a] Data are from single component adsorption experiments.

little or no affinity for the surface silanol groups present in the original MCM-41. NH_2-MCM-41 displays the highest adsorption capacity for gold of 0.40 mmol/g (79 mg/g) or roughly 0.40 mol of gold for each mole of amino grafted on the adsorbent. The adsorption capacities of NRH-MCM-41 and NR_2-MCM-41 are significantly lower with values of 0.33 (65 mg/g) and 0.20 mmol/g (40 mg/g), respectively. These values compare well with most gold adsorbents reported in the literature (Table 3). None of the four adsorbents adsorbed copper or nickel under the same experimental conditions. This shows that all amino-derived adsorbents are selective for gold adsorption, but their capacity diminishes as the substitution of propyl groups decreases the availability of the lone pair of electrons in nitrogen for adsorption. Unlike most common adsorbents such as activated carbons and inorganic oxides, the mesoporous silica adsorbents possess a well-defined surface that is fully accessible to the adsorbates. Introducing surface chemical moieties (i.e., RNH_2, R_2NH, and R_3N) creates heterogeneity on an otherwise uniform surface. The Freundlich adsorption model is therefore used to describe the adsorption of metal ions on these adsorbents. Figure 4 shows that the model and experiment are in excellent agreement.

The best adsorbent, NH_2-MCM-41, was selected for further studies. Figure 5a plots the gold adsorption on mesoporous silica adsorbents with different amino loadings. The adsorption isotherms fit the Freundlich equation (i.e., $q_e = KC_e^n$). The exponent term, n, is the same for the four amino loadings and has a calculated value of 0.125. The constant K increases linearly from 0.07 to 1.4 with increasing amount of surface amino groups. Figure 5b clearly shows the relationship between gold adsorption and the grafted amino groups. The adsorption capacity of NH_2-MCM-41 increases with the number of amino groups on the surface. The plot shows that adsorbents with less than 0.6 mmol of NH_2 groups per gram have a very low adsorption capacity. Roughly one gold atom was adsorbed for every three amino groups in these adsorbents, while the NH_2-MCM-41 with more than 0.6 mmol/g of NH_2 adsorbs about three gold atoms for every four surface amino groups.

The FTIR spectra in Figure 5c show that the IR signal (3747 cm^{-1}) for the surface silanols decreases with increasing amounts

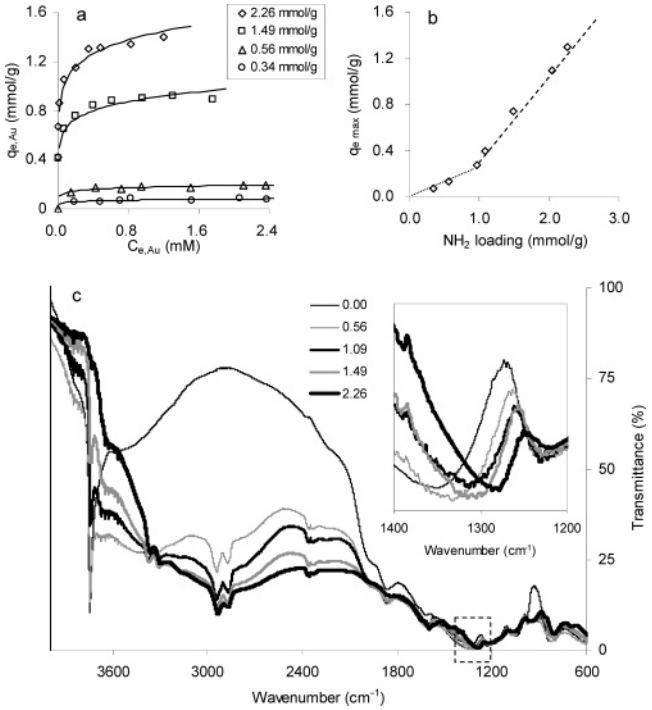

Figure 5. (a) Single component gold adsorption isotherms of NH_2-MCM-41 with different NH_2 loadings (0.1 g of adsorbent per 100 mL of solution, pH 2.5, and $T = 295 \pm 2$ K). (b) Plot of the maximum gold adsorption capacity as a function of the amount of surface amino groups on the NH_2-MCM-41 (0.22 mmol of NH_2 per 100 mL of solution, pH 2.5, and $T = 295 \pm 2$ K). (c) FTIR spectrum of NH_2-MCM-41 with different NH_2 loadings. The insert figure displays the peak shift caused by the interaction between the amino and surface silanol groups.

of grafted aminopropyl groups. It is evident from FTIR spectra that at low amino loadings there is a strong interaction between the terminal NH_2 of the aminopropyl groups and the unreacted surface silanol on MCM-41, which is revealed in the peak shift at around 1300 cm^{-1} in the spectra (Figure 5c, insert).[26] This may be responsible for the low gold adsorption of these samples. This effect disappears at amino loadings higher than 0.6 mmol/g, when most of the surface silanols were grafted with amino groups. Calculations indicated that even at the highest loading the average distance between the aminopropyls is larger than 1 nm. However, the actual distance is expected to be smaller since the unreacted methoxysilane groups in the grafted aminopropyl trimethoxysilane favor further deposition of the organic moieties at the immediate vicinity forming islands and patches of amino-derivatized areas instead of well-dispersed adsorption sites. This means that neighboring groups can interact with each other.

Binary-Components Separation. Figure 6 plots the equilibrium adsorption capacity of NH_2-MCM-41 adsorbent (2.26 mmol of NH_2/g) as a function of equilibrium gold concentration in the solution. The binary-components adsorption experiments were conducted by using solutions with equimolar metal ions concentrations at a fixed pH of 2.5 and temperature of 295 ± 2 K. Both parts a and b of Figure 6 show that only gold was adsorbed by NH_2-MCM-41 in complete exclusion of copper and nickel in the solutions. This means that 100% selectivity for gold was obtained under the experimental conditions. The maximum amounts of gold adsorbed by NH_2-MCM-41 are comparable, with a value of 1.05 mmol/g (200 mg/g) for both $AuCl_3/CuCl_2$ and $AuCl_3/Ni(NO_3)_2$ binary solutions. The LeVan and Vermeulen model,[27] derived from the Ideal Adsorption Solution (IAS) theory of Myer and Prausnitz,[28] was used to predict the binary adsorptions from the single-component adsorption data. Equation 1 is the simplified form of the LeVan and Vermeulen equation for the single-component Freundlich isotherm assuming that the Freundlich exponent, n, is the same for the two adsorbates.

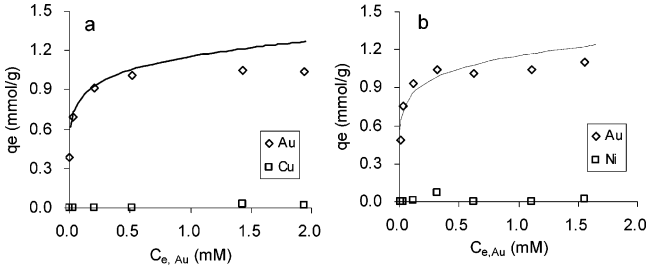

Figure 6. Plots of the effects of solution concentration on the (a) Au^{3+}/Cu^{2+} and (b) Au^{3+}/Ni^{2+} adsorption on NH_2-MCM-41 (2.2 mmol of NH_2/g of adsorbent, 0.1 g of adsorbent per 100 mL of solution, $[Au^{3+}]/[M^{2+}] = 1$, pH 2.5, and $T = 295 \pm 2$ K). Please note the symbols represent experimental data and the lines represent model calculation.

$$q_{e,1} = \frac{n\left(\frac{K_1}{n}\right)^{1/n} C_{e,1}}{\left[\left(\frac{K_1}{n}\right)^{1/n} C_{e,1} + \left(\frac{K_2}{n}\right) C_{e,2}\right]^{1-n}} \quad (1)$$

where $q_{e,1}$ is the amount of component 1 adsorbed at equilibrium; $C_{e,1}$ and $C_{e,2}$ are the equilibrium concentrations of components 1 and 2, respectively; and K_1 and K_2 are the values of Freundlich constants from the single-component adsorption isotherms of components 1 and 2, respectively. The effects of the anion were taken into account by using the published data on dissociation constants of the metal salts. The model parameters are listed in Table 4 and the model calculations are plotted in Figure 6a and b. It is clear that there is a good agreement between the model and experiment. According to the model, the lower gold adsorption capacity for the binary adsorption (i.e., 1.05 mmol/g) compared to the single-component

TABLE 4: Values of the Model Parameters

	equation	parameter	value
LeVan and Vermeulen equation[27]	$q_{e,1} = \frac{\left(n\frac{K_1}{n}\right)^{1/n} C_{e,1}}{\left[\left(\frac{K_1}{n}\right)^{1-n} C_{e,1} + \left(\frac{K_2}{n}\right)^{1/n} C_{e,2}\right]^{1/n}}$	K_{Au} K_{Cu} or K_{Ni} n	1.41 0 0.125
dissociation constant of metal salts[29]	$K_{A_mB_n} = \frac{[A_mB_n]}{[A]^m[B]^n}$	pK_{AuCl_3} pK_{CuCl_2} $pK_{Cu(NO_3)_2}$ pK_{NiCl_2} $pK_{Ni(NO_3)_2}$	29.6 0.1 0 0 –

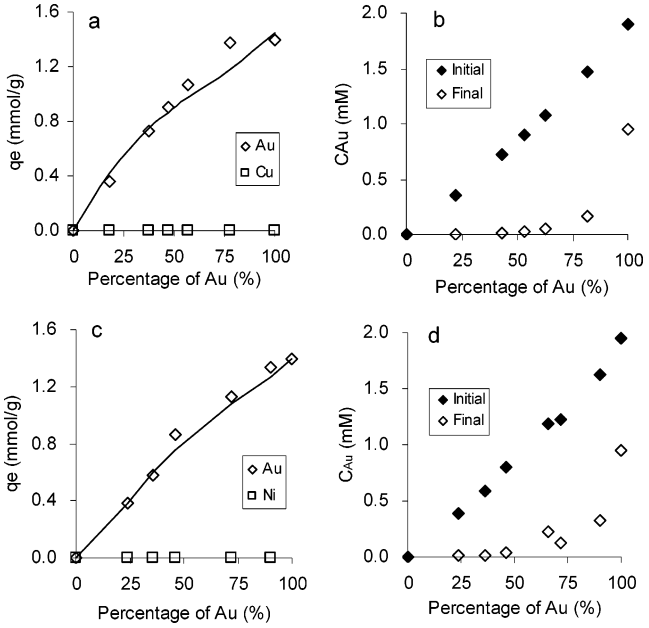

Figure 7. Plots of the effects of solution composition on the (a, b) Au^{3+}/Cu^{2+} and (c, d) Au^{3+}/Ni^{2+} adsorption on NH_2-MCM-41 (2.2 mmol of NH_2/g of adsorbent, 0.1 g of adsorbent per 100 mL of solution, $[Au^{3+}] + [M^{2+}] = 2$ mM, pH 2.5, and $T = 295 \pm 2$ K). Please note the symbols represent experimental data and the lines represent model calculation.

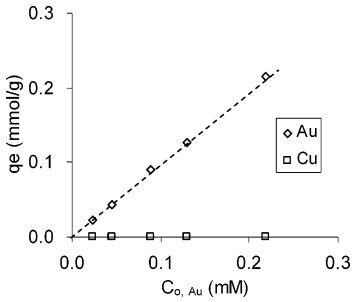

Figure 8. Adsorption of trace gold from the mixture containing a high concentration of copper (2.2 mmol of NH_2/g of NH_2-MCM-41, 0.1 g of adsorbent per 100 mL of solution, $[Cu^{2+}] = 1$ mM, pH 2.5, and $T = 295 \pm 2$ K). Please note the line was added to guide the eyes.

adsorption capacity of 1.4 mmol/g is due to the higher concentration of anions in the binary solution. The poorer fit observed for the $AuCl_3/Ni(NO_3)_2$ system is possibly due to interactions between the mixed chloride and nitrate ions that were not accounted for in the model.

Separate adsorption experiments were carried at a fixed total metal ions concentration of 2 mM, but with varying gold content of 0 to 100 mol %. The adsorption was allowed to reach equilibrium at constant temperature and pH. Parts a and c in Figure 7 show that the base metals copper and nickel are not adsorbed by NH_2-MCM-41 regardless of the starting composition of the solutions and only gold is adsorbed and removed. The model accurately predicted the adsorbed amount of gold. The plots of initial and final gold concentrations are displayed in parts b and d in Figure 7 for $AuCl_3/CuCl_2$ and $AuCl_3/Ni(NO_3)_2$ solutions, respectively. They show that the NH_2-MCM-41 adsorbent is capable of completely removing all gold from solutions of copper and nickel. For solutions containing large amounts of gold, the gold removal efficiency decreases as the adsorbent nears saturation. Figure 8 shows that NH_2-MCM-41 adsorbent is very efficient in removing trace amounts of gold from solutions containing mostly base metals such as copper. In the experiments, the concentration of $CuCl_2$ was kept at 1 mM, while the $AuCl_3$ concentration was varied from 0 to 0.25 mM. The results show that only gold was adsorbed even when the gold concentration in the solution was as low as 0.02 mM or 5 ppm. A 100% gold removal was obtained for the entire range of gold concentrations tested (i.e., 0.02 to 0.25 mM). It is possible to conclude that the excellent selectivity of NH_2-MCM-41 adsorbent for gold is not affected by the metal concentrations (i.e., Au^{3+}, Cu^{2+}, and Ni^{2+}) in the solution and complete gold removal by adsorption is possible even in solutions containing a very dilute amount of gold.

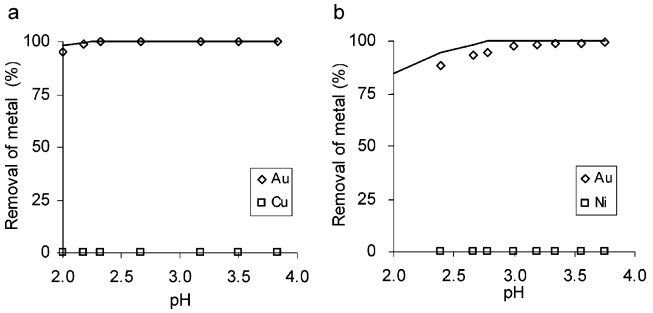

Figure 9. Plots of the effects of pH on the adsorption properties of NH_2-MCM-41 for (a) Au^{3+}/Cu^{2+} and (b) Au^{3+}/Ni^{2+} solutions (2.2 mmol of NH_2/g of adsorbent, 0.1 g of adsorbent per 100 mL of solution, $[Au^{3+}] = [M^{2+}] = 1$ mM and $T = 295 \pm 2$ K). Please note the symbols represent experimental data and the lines represent model calculation.

The effects of pH on gold adsorption from the binary solutions were investigated and the results are shown in Figure 9. The study was conducted between pH 2 and 4. The solution pH was adjusted by adding hydrochloric acid (HCl). According to Murphy,[30] only $AuCl_4^-$ exists at pH lower than 4 and the $Au(OH)_xCl^-_{4-x}$ species ($x = 1$ to 4) are absent at these pH values. The gold adsorption was low when the pH was lower than 2 while the metal solution becomes unstable and gold metal precipitates at pH higher than 4, which is in agreement with the result from Ghosh et al.[31] Neither copper nor nickel was adsorbed at this pH range and gold was the only metal adsorbed by NH_2-MCM-41. The adsorption capacity of NH_2-MCM-41 is affected by the pH and shows a decreasing trend with lower pH. The model gives an accurate prediction of the gold adsorption at different pH values by simply accounting for the effect of higher concentration of chloride ions from the addition of HCl on the dissociation of metal salts. The ζ potential measurement indicated that NH_2-MCM-41 has an isoelectric point at a pH of 3, and at pH values lower than this value, the amino group is protonated and the surface of the adsorbent is positively charged. The presence of other ionic species is known to affect the isoelectric point, but it is sufficient to say that the protonated $^+NH_3$-MCM-41 found at low pH values is less able to accommodate the adsorption of Au^{3+} ions. Both experiment and model suggest that it may be possible to recover the adsorbed gold ions and regenerate the adsorbent by a simple acid wash.

Gold Recovery and Adsorbent Regeneration. The feasibility of gold removal and recovery from very dilute gold solution was investigated. A 0.05-g sample of NH_2-MCM-41 was added to a 500-mL solution containing 0.05 mM $AuCl_3$ and 1 mM $CuCl_2$. Complete gold removal from the solution was obtained after 24 h of adsorption (Figure 10a), and the remaining solution contained only copper. XPS analysis of the spent adsorbent found only the signal from gold and not copper, confirming that copper was not adsorbed by NH_2-MCM-41. On the basis of model calculation, all the adsorbed gold could be recovered at 5 M HCl. The spent adsorbent was washed with 3 mL of 5.2 M HCl for 5 min to recover a 2 mM pure $AuCl_3$ solution, which

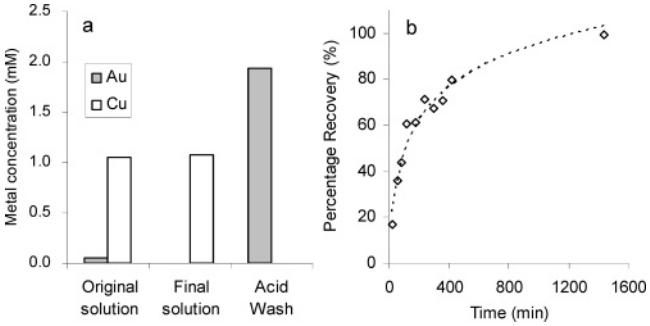

Figure 10. (a) Plots of metal concentrations in the original gold−copper solution before and after adsorption and in the wash solution after adsorbent regeneration (2.2 mmol of NH_2/g of NH_2-MCM-41, 0.1 g of adsorbent per 1000 mL of solution, $[Au^{3+}] = 0.05$ mM, $[Cu^{2+}] = 1$ mM, pH 2.5, and $T = 295 \pm 2$ K). (b) Percent gold recovered from spent adsorbent as a function of washing time. Please note the line was added to guide the eyes.

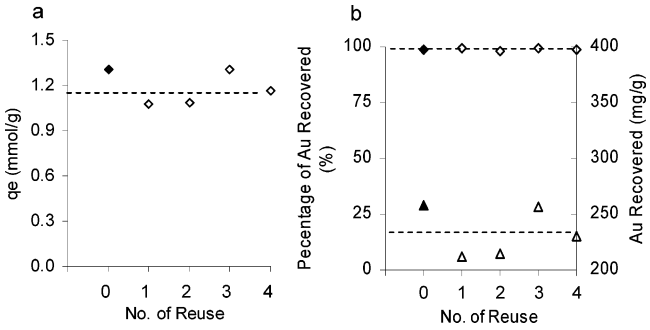

Figure 11. (a) Plots of adsorption capacity and (b) gold recovery from NH_2-MCM-41 after repeated adsorption and regeneration experiments (2.2 mmol of NH_2/g of NH_2-MCM-41, 0.125 g of adsorbent per 100 mL of solution, $[Au^{3+}] = [Cu^{2+}] = 3$ mM, pH 2.5, and $T = 295 \pm 2$ K). Please note the line was added to guide the eyes.

is 40× more concentrated that the original solution. More adsorbed gold is recovered at longer washing time as shown in Figure 10b. Complete recovery of adsorbed gold was obtained after 24 h. It is expected that washing time can be shorter, once the washing procedure is optimized.

Figure 11 summarizes the results of gold recovery and adsorbent regeneration experiments. Fresh NH_2-MCM-41 was used to adsorb gold from a solution containing 3 mM $AuCl_3$ and 3 mM $CuCl_2$. Gold (1.3 mmol/g; 256 mg/g) was adsorbed (Figure 11a) in an amount close to the maximum adsorption capacity of the adsorbent. Analysis showed that no copper was adsorbed and only gold was removed from the solution. The saturated adsorbent was washed with 5.2 M HCl solution for 24 h, recovering more than 99% of the adsorbed gold. The recovered gold solution was at least 99.9% pure. The regenerated adsorbent was washed with distilled water and reused for adsorption. Figure 11b shows that the regenerated adsorbent maintained its adsorption capacity even after repeated use. The excellent adsorption selectivity remained unchanged and only gold was adsorbed in each reuse. All gold was successfully recovered from the spent adsorbent by acid wash as shown in Figure 11b.

Concluding Remarks

Surface organic amines including propylamine, dipropylamine, and tripropylamine groups display strong affinity for gold adsorption. Facile removal and recovery of high-purity gold from mixtures was successfully accomplished by using a gold-selective and regenerable adsorbent prepared by grafting propylamines on mesoporous MCM-41. The NH_2-MCM-41 adsorbed only gold, not the other metals (i.e., copper and nickel) in the solution. The 100% selectivity for gold was maintained, regardless of the solution concentration, composition, and pH (i.e., 2 to 4). Gold in as little as 5 ppm was completely removed by the adsorbent from solutions containing as high as 150 ppm of copper or nickel. This is important, as precious metals in wastewater are usually present in low concentrations. The adsorption was also rapid as the MCM-41 has large, easily accessible pores. The adsorbed gold was completely recovered by a simple acid wash and the recovered gold solution was better than 99% pure. The regenerated adsorbent exhibited the same adsorption capacity and selectivity as the fresh adsorbent even after being reused several times.

The MCM-41's simple cylindrical pore geometry and well-defined surface approach the ideal surface assumed in most adsorption models. Grafting surface chemical moieties (i.e., RNH_2, R_2NH, and R_3N) introduces heterogeneity on an otherwise uniform surface. The Freundlich adsorption model best describes metal adsorption on these adsorbents. The LeVan and Vermeulen model based on the single-component Freundlich isotherm provided an accurate description of the binary adsorption process on the mesoporous silica adsorbents after taking into account the anion effect. We are able to fit the data using the simple model with minimum correction, which accounts for the anion effect. It will be indispensable for the scale-up of the adsorption process. Indeed, it served as an important guide in designing the gold recovery and adsorption regeneration processes described in this work.

Acknowledgment. The authors gratefully acknowledge the funding from the Hong Kong Research Grant Councils (grant RGC-HKUST 6037/00P). We thank the Material Characterization and Preparation Facility at the HKUST for the use of XRD, SEM, TEM, XPS, and TGA/DTA equipment and the Advanced Engineering Material Facility for the use of the Coulter SA3100 surface area and pore size analyzer and the Beckman Coulter Zeta-Potential analyzer.

References and Notes

(1) Taguchi, A.; Schuth, F. *Microporous Mesoporous Mater.* **2005**, *77*, 1.
(2) Somorjai, G. A.; Rioux, R. M. *Catal. Today* **2005**, *100* (3−4), 201.
(3) Brunel, D.; Blanc. A. C.; Galarneau, A.; Fajula, F. *Catal. Today* **2002**, *73*, 139.
(4) Hata, H.; Saeki, S.; Kimura, T.; Sugahara, Y.; Kuroda, K. *Chem. Mater.* **1999**, *11*, 1110.
(5) Feng, X.; Fryxell, G. E.; Wang, L.-Q.; Kim, A. Y.; Liu, J.; Kemmer, K. M. *Science* **1997**, *276*, 923.
(6) Ho, K. Y.; McKay, G.; Yeung, K. L. *Langmuir* **2003**, *19*, 3019−3024.
(7) Meltzer, M.; Callahan, M.; Jensen, T. *Metal-bearing waste streams: minimizing, recycling and treatment*; Noyes Data Corp.: Park Ridge, NJ, 1990.
(8) Patra, M.; Bhowmik, N.; Bandopadhyay, B.; Sharma, A. *Environ. Exp. Bot.* **2004**, *52*, 199.
(9) Baldwin, R. D.; Marshall, J. W. *Ann. Clin. Biochem* **1999**, *36*, 267.
(10) Kakkar, P.; Jaffery, F. N. *Environ. Toxicol. Pharmacol.* **2005**, *19*, 335.
(11) Cheremisinoff, P. N. *Encyclopedia of Environmental Control Technology*; Vol. 3, Wastewater Treatment Technology; Gulf Publishing Company: Houston, TX, 1989; p 543.
(12) Olkhovyk, O.; Antochshuk, V.; Jaroniec, M. *Colloids Surf. A* **2004**, *236*, 69.
(13) Aguado, J.; Arsuaga, J. M.; Arencibia, A. *Ind. Eng. Chem. Res.* **2005**, *44*, 3665.
(14) Brown, J.; Mercier, L.; Pinnavaia T. J. *Chem. Commun.* **1999**, 69.
(15) Fryxell, G. E.; Liu, L.; Hauser, T. A.; Nie, Z.; Ferris, K. F.; Mattigod, S.; Gong, M.; Hallen, R. T. *Chem. Mater.* **1999**, *11*, 2148.
(16) Kang, T.; Park, Y.; Choi, K.; Lee, J. S.; Yi, L. *J. Mater. Chem.* **2004**, *14*, 1043.

(17) Kruk, M.; Jaroniec, M.; Sayari, A. *Chem. Mater.* **1999**, *11*, 492.
(18) Nakbanpote, W.; Thiravetyan, P.; Kalambaheti, C. *Miner. Eng.* **2002**, *15*, 549.
(19) Kongolo, K.; Kinabo, C.; Bahr, A. *Hydrometallurgy* **1997**, *44*, 191.
(20) Syna, N.; Valix, M. *Miner. Eng.* **2003**, *16*, 421.
(21) Sanchez, J. M.; Hidalgo, M.; Valiente, M.; Salvado, V. *J. Polym. Sci. Part A: Polymer Chemistry* **2000**, *38*, 269.
(22) Gomes, C. P.; Almeida, M. F.; Loureiro, J. M. *Sep. Purif. Technol.* **2001**, *24*, 35.
(23) Nakbanpote, W.; Thiravetyan, P.; Kalambahetf, C. *Miner. Eng.* **2000**, *13*, 391.
(24) Mensah-Biney, R.; Reid, K. J.; Hepworth, M. T. *Miner. Eng.* **1995**, *8*, 125.
(25) Donia, A. M.; Atia, A. A.; Elwakeel, K. Z. *Sep. Purif. Technol.* **2005**, *42*, 111.
(26) Azour, H.; Derouault, J.; Lauroua, P.; Vezon, G. *Spectrochim. Acta, Part A* **2000**, *56*, 1627.
(27) LeVan, M. D.; Vermeulen, T. *J. Phys. Chem.* **1981**, *85*, 3247.
(28) Myer A. L.; Prausnitz, J. M. *AIChE J.* **1965**, *11* (1), 121.
(29) Martell, A. E.; Smith, R. M. *Critical Stability Constants*; Plenum Press: NY, 1974.
(30) Murphy, P. J.; Lagrange, M. S. *Geochim. Cosmochim. Acta* **1998**, *62* (21−22), 3515.
(31) Ghosh, A.; Patra, C. R.; Mukherjee, P.; Sastry, M.; Kumar, R. *Microporous Mesoporous Mater.* **2003**, *58*, 201.